Supporting Information

Modulation of Phosphorene for Optimal Hydrogen Evolution Reaction

*Jiang Lu[‡1], Xue Zhang[‡1], Danni Liu[‡1], Na Yang[1], Hao Huang[1], Shaowei Jin[2], Jiahong Wang[*1,3], Paul K. Chu[3], Xue-Feng Yu[1]*

[1]Shenzhen Institutes of Advanced Technology, Chinese Academy of Sciences, Shenzhen 518055, P. R. China

[2]National Supercomputing Center, Shenzhen, Guangdong 518055, P. R. China

[3]Department of Physics, Department of Materials Science and Engineering, and Department of Biomedical Engineering, City University of Hong Kong, Tat Chee Avenue, Kowloon, Hong Kong, China

* Corresponding Author: jh.wang1@siat.ac.cn

‡ These authors contributed equally to this work

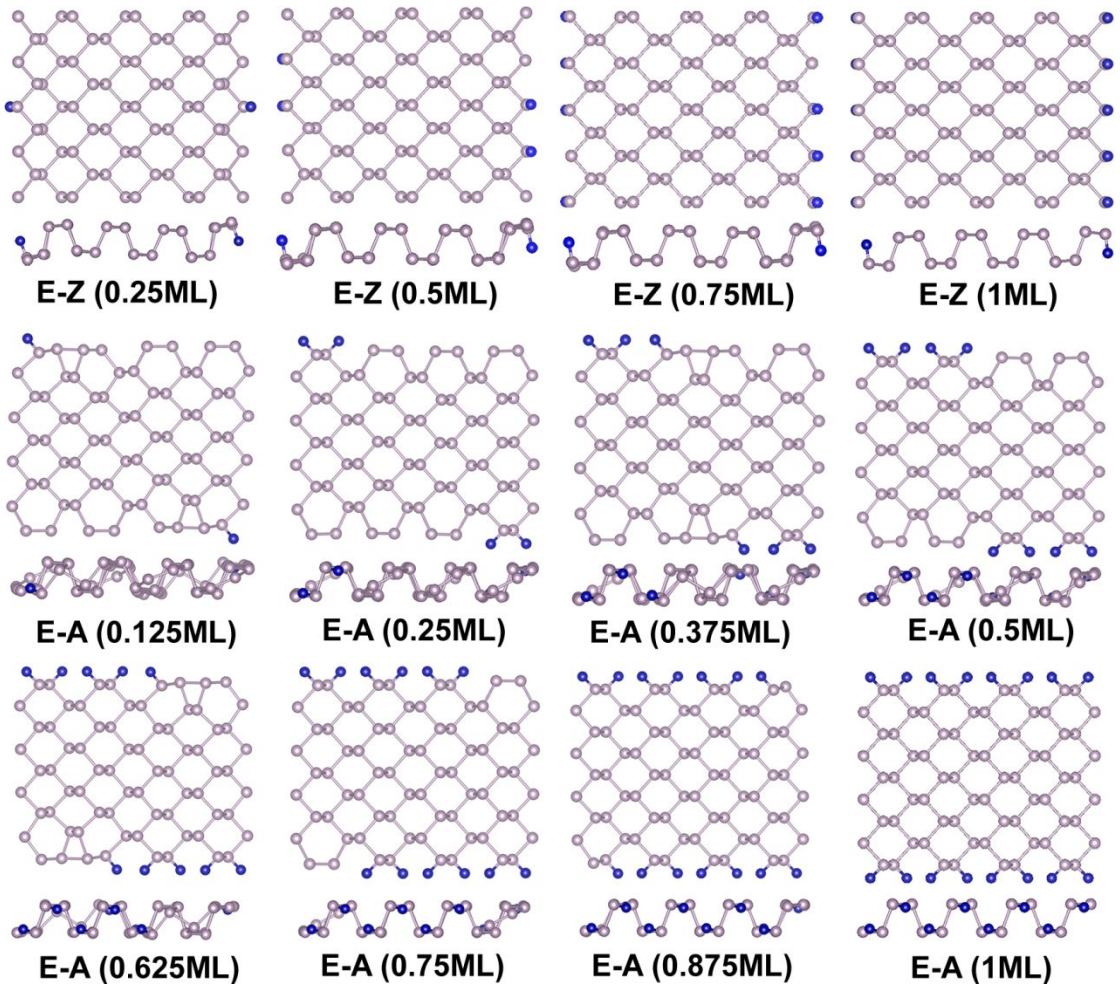

Figure S1. Reconstruction of BP edges (E-Z, E-A) with different hydrogen coverages.

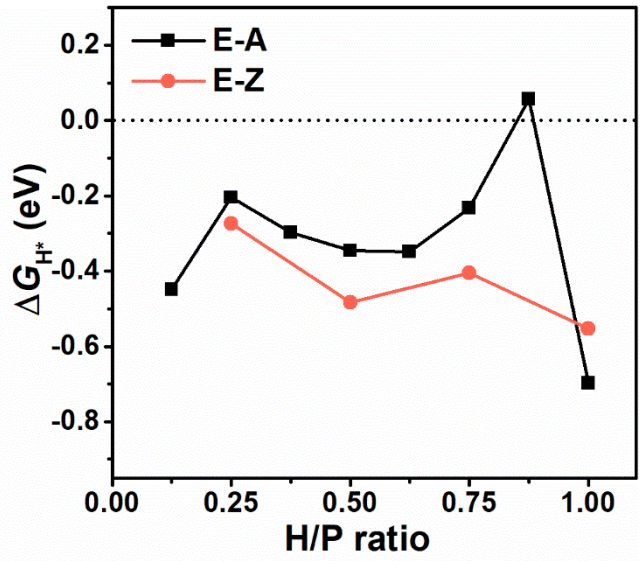

Figure S2. The Gibbs free energies (ΔG_{H^*}) for E-Z and E-A edges at different hydrogen coverage.

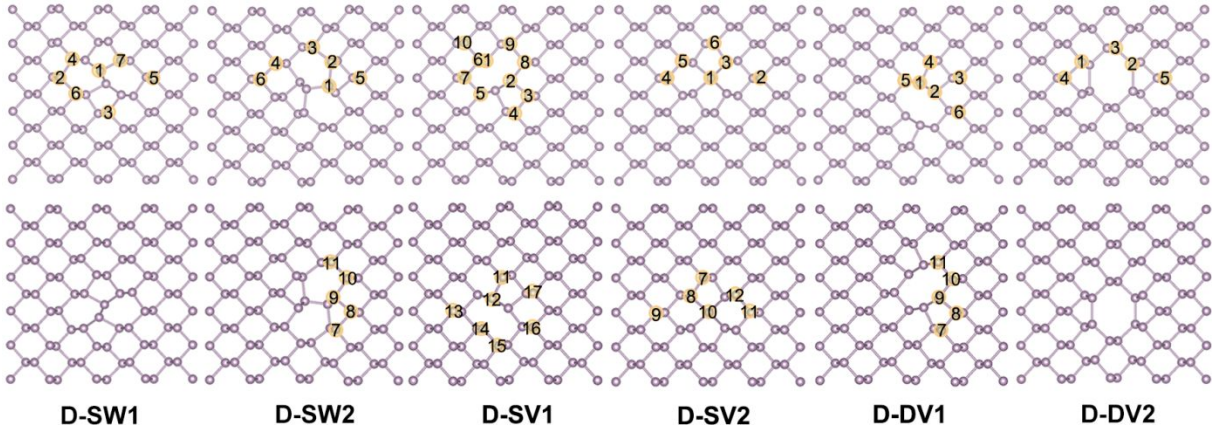

Figure S3. Atomic structures of the phosphorene defects (D-SW1, D-SW2, D-SV1, D-SV2, D-DV1, D-DV2) with the adsorption sites labeled in the front side (upper) and back side (lower). Note that the adsorption sites of front and back side is equal for two defects (D-SW1 and D-DV2).

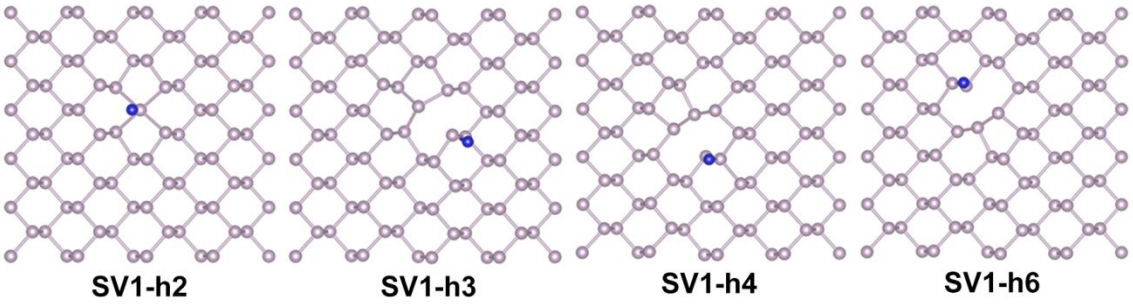

Figure S4. Four optimized structures of D-SV1 models after H adsorption.

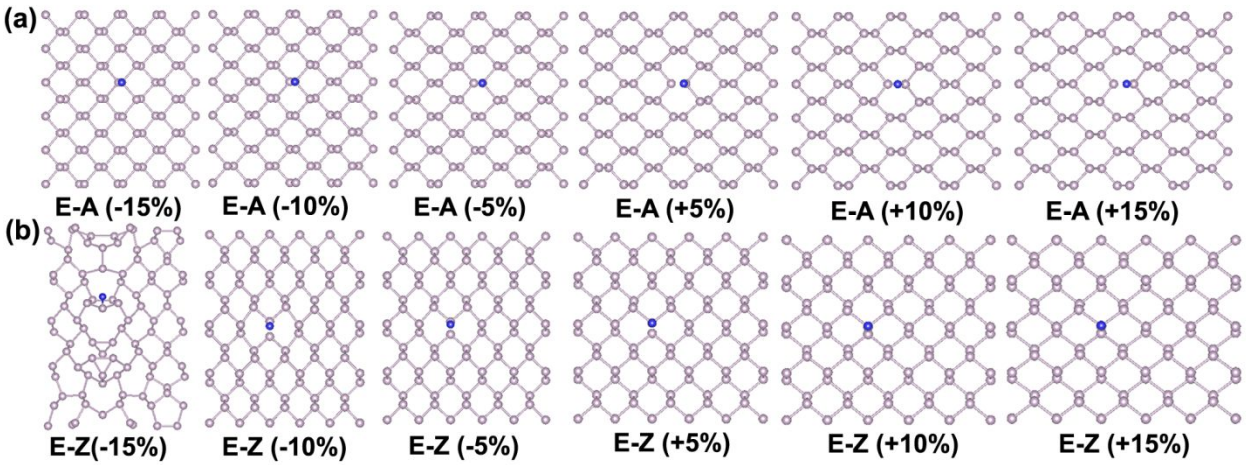

Figure S5. Optimized structures of strained BP after H adsorption. (a) Straining along Armchair (E-A) direction; (b) Straining along Zigzag (E-Z) direction;

Note: E-Z (-15%) model is unstable when H adsorbed and this result is ignored in this work.

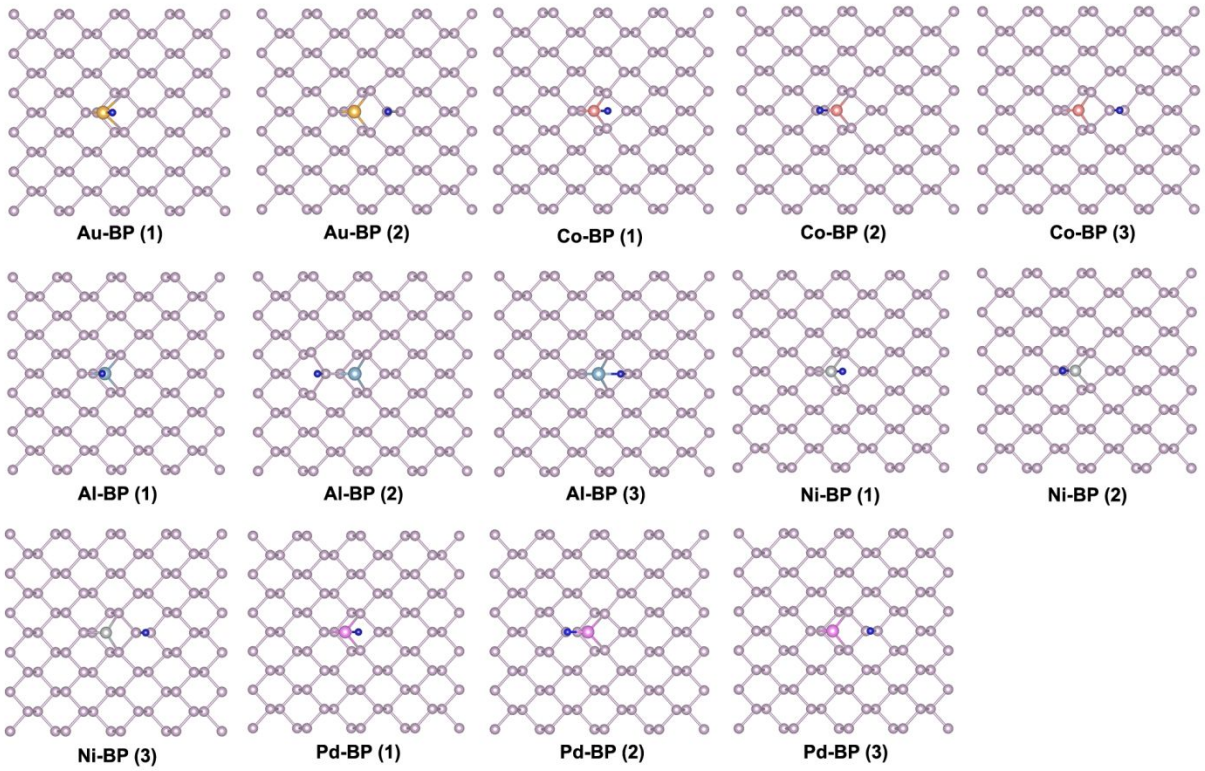

Figure S6. Typical adsorption sites of H atom at Metal-doped BP.

Table S1. The ΔG_{H^*} values of the H* adsorbed on all the possible sites of different models.

Models	Site (Coverage)	ΔE_{H^*}/eV	ΔG_{H^*}/eV	Models	Site (Coverage)	ΔE_{H^*}/eV	ΔG_{H^*}/eV
B	**1**	**0.95**	**1.24**		14	-0.71	-0.42
E-A	0.125 ML	-0.74	-0.45		15	-0.13	0.16
	0.25 ML	-0.49	-0.20		16	0.34	0.63
	0.375 ML	-0.59	-0.30		17	0.24	0.53
	0.5 ML	-0.64	-0.35	D-SV2	1	-0.64	-0.35
	0.625 ML	-0.64	-0.35		2	0.07	0.36
	0.75 ML	-0.52	-0.23		3	-1.02	-0.73
	0.875 ML	**-0.23**	**0.06**		4	0.02	0.31
	1 ML	-0.99	-0.70		5	-0.11	0.18

E-Z	**0.25 ML**	**-0.56**	**-0.27**		**6**	**-0.43**	**-0.14**
	0.5 ML	-0.77	-0.48		7	-0.12	0.17
	0.75 ML	-0.70	-0.41		8	-0.58	-0.29
	1 ML	-0.84	-0.55		9	0.10	0.39
D-SW1	1	1.15	1.44		10	-0.63	-0.34
	2	0.92	1.21		11	-0.03	0.26
	3	1.00	1.29		12	-0.52	-0.23
	4	1.01	1.30	D-DV1	**1**	**0.10**	**0.39**
	5	1.00	1.29		2	0.27	0.56
	6	0.64	0.93		3	0.86	1.15
	7	**0.59**	**0.88**		4	0.77	1.06
D-SW2	1	0.53	0.82		5	1.68	1.97
	2	0.72	1.01		6	1.02	1.31

	3	**0.42**	**0.71**		7	0.90	1.19
	4	1.02	1.31		8	0.70	0.99
	5	0.66	0.95		9	0.24	0.53
	6	0.81	1.10		10	0.65	0.94
	7	0.82	1.11		11	0.56	0.85
	8	0.63	0.92	D-DV2	1	0.26	0.55
	9	0.60	0.89		**2**	**-0.31**	**-0.02**
	10	0.77	1.06		3	0.21	0.50
	11	0.79	1.08		4	0.47	0.76
D-SV1	1	-0.73	-0.44		5	0.84	1.13
	2	**-0.28**	**0.01**	S-A	**-15%**	**0.31**	**0.60**
	3	-0.19	0.10		-10%	0.70	0.99
	4	-0.12	0.17		-5%	0.90	1.19

5	0.11	0.40		5%	0.97	1.26
6	-0.12	0.17		10%	0.80	1.09
7	0.18	0.47		15%	0.62	0.91
8	0.20	0.49	S-Z	**-10%**	**0.72**	**1.01**
9	0.12	0.41		-5%	0.94	1.23
10	0.11	0.40		5%	0.96	1.25
11	-0.71	-0.42		10%	0.86	1.15
12	0.14	0.43		15%	0.78	1.07
13	0.24	0.53				

Note: S-Z and S-A respect strain in armchair and zigzag direction, respectively.

Table S2. The ΔE_{H^*}, E_{ZPE-H}, ΔE_{ZPE}, $\Delta E_{ZPE} - T\Delta S$ and ΔG_{H^*} values of the H* adsorbed on the typical P site of different models.

Models	Site	ΔE_{H^*}/eV	E_{ZPE-H}/eV	ΔE_{ZPE}/eV	($\Delta E_{ZPE} - T\Delta S$)/eV	ΔG_{H^*}/eV
B	1	0.95	0.21	0.08	**0.28**	1.24
E-A	0.125 ML	-0.74	0.23	0.09	**0.29**	-0.44
E-Z	0.25 ML	-0.56	0.22	0.09	**0.29**	-0.27
D-1	2	0.92	0.21	0.08	**0.28**	1.20
D-2	3	0.42	0.22	0.08	**0.28**	0.70
D-3	2	-0.28	0.23	0.09	**0.30**	0.02
D-4	5	-0.11	0.23	0.09	**0.30**	0.18
D-5	1	0.10	0.22	0.08	**0.29**	0.39
D-6	2	-0.31	0.22	0.09	**0.29**	-0.02

Note: ($\Delta E_{ZPE} - T\Delta S$) is calculated 0.29 (± 0.01) eV, that is $\Delta G_{H^*} = \Delta E_{H^*} + 0.29$ eV, which was then used in all the conversion relation of different models.

Table S3. The ΔE_{H^*}, $E_{ZPE\text{-}H}$, ΔE_{ZPE}, $\Delta E_{ZPE} - T\Delta S$ and ΔG_{H^*} values of the H* adsorbed on the typical P site of doped-BP models.

Models	Site	ΔE_{H^*}/eV	$E_{ZPE\text{-}H}$/eV	ΔE_{ZPE}/eV	(ΔE_{ZPE} – TΔS)/eV	ΔG_{H^*}/eV
Au-BP	1	-0.80	0.18	0.05	0.25	-0.54
	2	0.80	0.18	0.05	0.25	1.06
Co-BP	1	-0.16	0.18	0.05	0.25	0.09
	2	0.20	0.15	0.01	0.22	0.41
	3	0.43	0.22	0.09	0.29	0.72
Al-BP	1	-0.04	0.17	0.03	0.24	0.20
	2	0.43	0.23	0.09	0.30	0.73
	3	0.65	0.15	0.02	0.22	0.87
Ni-BP	1	0.40	0.16	0.03	0.23	0.63

	2	0.63	0.15	0.01	0.22	0.85
	3	1.15	0.19	0.06	0.26	1.41
Pd-BP	1	0.65	0.17	0.03	0.24	0.88
	2	1.04	0.14	0.01	0.21	1.25
	3	1.14	0.20	0.06	0.27	1.40

Note: We've tested all the typical sites around the doped atom on the BP surface, and selected the above typical sites with some replicate results removed.

Experimental Section

1. Preparation of large black phosphorene (L-BP) sheets and small black phosphorene (S-BP) sheets

Typically, large black phosphorene (L-BP) sheets with 10 μm lateral dimension were obtained by a simple electrochemical prepared process in a two-electrode setup by direct-current power supply, where Pt foil (1 cm × 1 cm × 0.1 cm) was chosen as

positive electrode, black phosphorus (BP) crystal (0.5 cm × 0.5 cm × 0.1 cm) was used as negative electrode and N,N-dimethylformamide (DMF) contained 5 mM Tetra-n-octylammonium bromidectrode was used as electrolyte. BP crystal was expanded by applying voltage at 10 V for 20 min and then dispersed in N,N-Dimethylformamide (DMF) by sonication for 20 min. The result L-BP sheets dispersion was let to stand 30 min to remove thick-layered BP, and then washed by ethanol at least three times used centrifuged at 9000 rpm for 10 min to get thin layered BP sheets ethanol dispersion. Small black phosphorene (S-BP) sheets with 1 μm lateral dimension were prepared by similar method only changed applying voltage as 20 V.

2. Preparation of Co doped black phosphorene (L-$BP_{(Co)}$) sheets

Co doped phosphorene (L-$BP_{(Co)}$) sheets were synthesized via a facile hydrothermal reaction, $CoCl_2$ (1 mmol) and urea (3 mmol) were dissolved in 40 mL BP sheets DMF dispersion under vigorous stirring for 30 min. Then the solution was transferred to a 50 mL Teflon-lined stainless-steel autoclave, sealed and maintained at 180 °C for 1 h in an electric oven. After the autoclave cooled

down at room temperature, the solution was collected and washed by ethanol several times centrifuged at 9000 rpm for 10 min to obtain L-$BP_{(Co)}$ sheets ethanol dispersion.

3. Characterizations

Scanning electron microscopy (SEM) measurements were performed on Zeiss Supra 55 scanning electron microscope at an accelerating voltage of 2 kV. X-ray diffraction (XRD) data were acquired on a Bruker D2 X-ray diffractometer with Cu Kα radiation (k = 1.5418 Å). The X-ray photoelectron spectroscopy (XPS) measurements were carried out on a Thermo Fisher ESCALAB 250Xi XPS. Raman scattering was performed on a Horiba Jobin-Yvon Lab Ram HR VIS high-resolution confocal Raman microscope equipped with a 532 nm laser as the excitation source at room temperature.

4. Electrode Preparation

Prior to modification, the glassy carbon electrodes (GCE, 3 mm in diameter) were respectively polished with alumina slurry, and cleaned by ultrapure water, then dried by nitrogen. The concentration of the ethanol dispersions of L-BP, S-BP, L-$BP_{(Co)}$, and Pt/C was tuned as 100 μg mL^{-1}, respectively. 990 μL dispersion with 10 μL Nafion

solution (0.05 wt %) were sonicated for 3 min to form an ink. Afterwards, 10 μL of the ink were loaded onto the cleared GCE and dried at room temperature.

5. Electrochemical measurements

All Electrochemical results were obtained in a standard three-electrode setup by CHI 760E electrochemical analyzer (CH Instruments, Inc., Shanghai) at ambient temperature using GCE as working electrode, a graphite rod as counter electrode and a saturated calomele electrode (SCE) as the reference electrode. For all measurements, the obtained potential was calibrated with respect to reversible hydrogen electrode (RHE) as formula, E(RHE) = E(SCE) + (0.059 pH + 0.242) V. Cyclic voltammogram curves were obtained by cyclic voltammetry from -0.043 to 0.087 V vs RHE at scan rate of 5, 50, 100, 150, 200 mV s^{-1} where there was no Faradic current. The double-layer capacitance can be calculated as formula, C_{dl} = j/r, where j was the current density and r was the scan rate. Electrochemically active surface area (EASA) can be calculated as: $EASA = C_{dl}/C_s$, where C_s was the specific capacitance value for a flat standard with 1 cm^2 of real surface area. The general

value of C_s was between 20 μF cm^{-2} and 60 μF cm^{-2}. Here, 60 μF cm^{-2} was used as the average value. Linear sweep voltammetry was performed to get polarization curves from 0 to -0.8 V with a scan rate of 2 mV s^{-1} in 0.5 M H_2SO_4. Before evaluate the HER activity of all result product, Pt/C (20%) with same loading mass was tested firstly to detect the measurement system. IR compensation was applied for all polarization curves by impedance measurements.

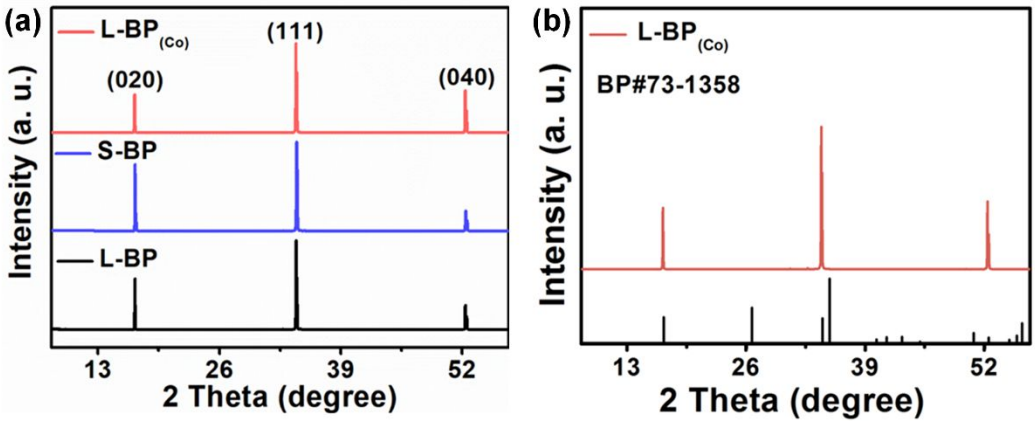

Figure S7. (a) XRD patterns of L-BP, S-BP and L-BP$_{(Co)}$. (b) The magnified XRD patterns of L-BP(Co).

As shown in **Figure S7**, L-BP and S-BP show diffraction peaks characteristic of BP (JCPDS No.73-1358). After Co doping, L-BP$_{(Co)}$ shows typical diffraction peaks of BP without signals belong to cobalt or cobalt compound.

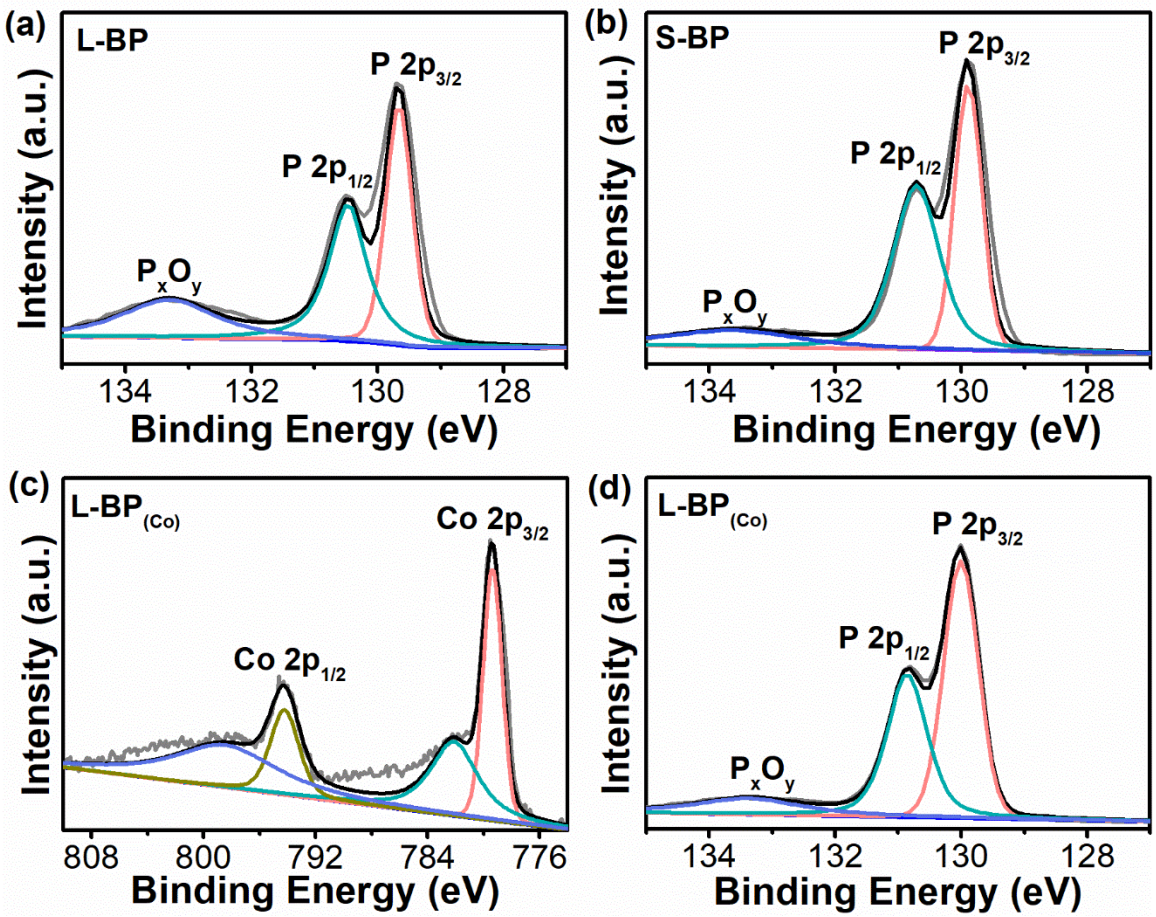

Figure S8. (a) P 2p XPS spectrum of L-BP. (b) P 2p XPS spectrum of S-BP. (c, d) Co 2p and P 2p XPS spectra of L-$BP_{(Co)}$, respectively.

Figure S8 display the X-ray photoelectron spectroscopy (XPS) spectra of L-BP, S-BP and L-$BP_{(Co)}$. The binding energies (BEs) of P $2p_{1/2}$ and P $2p_{3/2}$ of L-BP, S-BP and L-$BP_{(Co)}$ appear at 129.1 and 130.2 eV, respectively, consistent with the characteristic of

BP. After doped Co, the L-$BP_{(Co)}$ shows two peaks at 779.0 and 793.9 eV corresponding to Co $2p_{3/2}$ and Co $2p_{1/2}$, respectively.

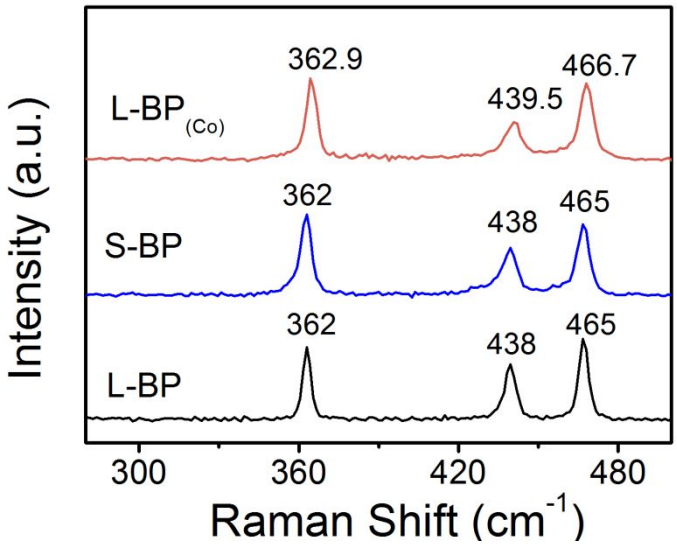

Figure S9. Raman scattering spectra of the L-BP, S-BP and L-BP(Co).

Figure S9 shows the Raman spectra of L-BP, S-BP and L-$BP_{(Co)}$. The Raman peaks of L-BP and S-BP locate at same position and the Raman peaks of L-$BP_{(Co)}$ red-shift slightly.

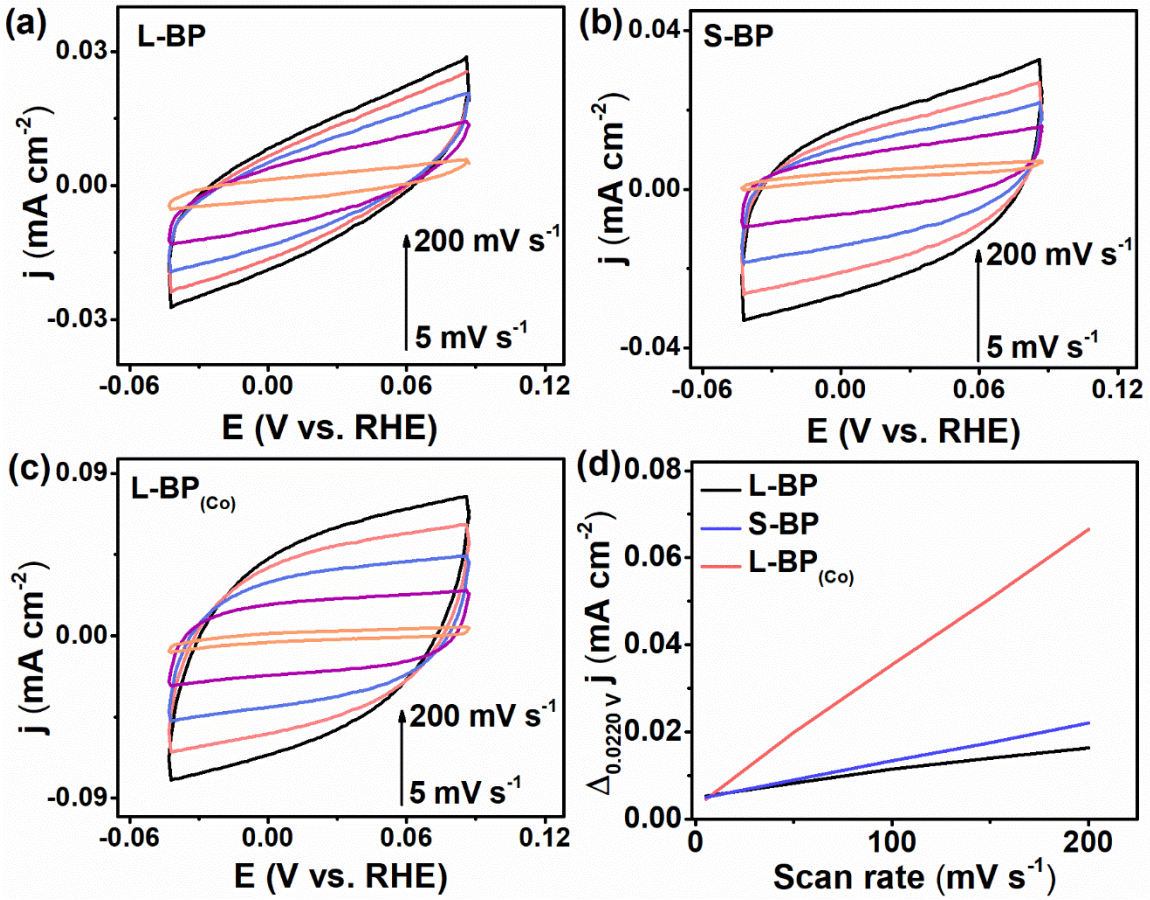

Figure S10 (a-c) CV conducted at potential from -0.043 to 0.087 V vs RHE at scan rates of 5, 50, 100, 150 and 200 mV s^{-1}. (d) The capacitive currents at 0.022 V as a function of scan rate for L-BP, S-BP and L-$BP_{(Co)}$ [$\Delta j_0 = 1/2 (j_a - j_c)$].

To assess the EASA of L-BP, S-BP and L-$BP_{(Co)}$, the CV cycles was measured at different scan rates during the potential from -0.043 to 0.087 V vs RHE, where there is

no Faradic current. The EASA of L-BP, S-BP and L-$BP_{(Co)}$ are 0.071, 0.10 and 0.36 cm^2, respectively.

Table S4. Comparison of the HER performance of this work and previous jobs

Ref	Catalysts	Electrolyte	Overpotential	Onset Overpotential (mV)	Tafel Slope (mV dec^{-1})
S1	NH_2-BP	1.0 M KOH	290 mV@10 mA cm^{-2}	N/A	63
S2	Ni_2P@BP	0.5 M H_2SO_4	107 mV@10 mA cm^{-2}	N/A	38.6
	BP	0.5 M H_2SO_4	600 mV@10 mA cm^{-2}	N/A	N/A
S3	MoS_2−BP nanosheet	0.5 M H_2SO_4	85 mV@10 mA cm^{-2}	85	68
	BP	0.5 M H_2SO_4	N/A	N/A	161
S4	BP/Co_2P	0.5 M H_2SO_4	340 mV@100 mA cm^{-2}	105	62
	BP	0.5 M H_2SO_4	600 mV@0.3 mA cm^{-2}	389	125
	BP/Co_2P	1.0 M KOH	336 mV@10 mA cm^{-2}	173	72
S5	EBP@1:4	1.0 M KOH	191 mV@100 mAcm^{-2}	N/A	76
	EBP@1:8	1.0 M KOH	210 mV@100 mA cm^{-2}	N/A	N/A
	EBP	1.0 M KOH	370 mV@10 mA cm^{-2}	N/A	135
S6	$BP_{(Co)}$	0.5 M H_2SO_4	294 mV@10 mA cm^{-2}	N/A	107
S7	BPQDs/Mxene	N/A	N/A	190	83
This work	L-$BP_{(Co)}$	0.5 M H_2SO_4	389 mV@20 mA cm^{-2}	194	47
	L-BP	0.5 M H_2SO_4	615 mV@20 mA cm^{-2}	355	91
	S-BP	0.5 M H_2SO4	511 mV@20 mA cm^{-2}	299	85

References

S1. Shao, L. Y.; Sun, H. M.; Miao, L. C.; Chen, X.; Han, M.; Sun, J. C.; Liu, S.; Li, L.; Cheng, F. Y.; Chen, J. Facile Preparation of NH_2-Functionalized Black Phosphorene for the Electrocatalytic Hydrogen Evolution Reaction. J. Mater. Chem. A 2018, 6, 2494-2499

S2. Luo, Z. Z.; Zhang, Y.; Zhang, C. H.; Tan, H. T.; Li, Z.; Abutaha, A.; Wu, X. L.; Xiong, Q. H.; Khor, K. A.; Hippalgaonkar, K.; Xu, J. W.; Hng, H. H.; Yan, Q. Y. Multifunctional 0D-2D Ni2P Nanocrystals-Black Phosphorus Heterostructure. Adv. Energy Mater. 2017, 7, 1601285.

S3. He, R.; Hua, J.; Zhang, A. Q.; Wang, C. H.; Peng, J. Y.; Chen, W. J.; Zeng, J. Molybdenum Disulfide-Black Phosphorus Hybrid Nanosheets as a Superior Catalyst for Electrochemical Hydrogen Evolution. Nano Lett. 2017, 17, 4311-4316.

S4. Wang, J. H.; Liu, D. N.; Huang, H.; Yang, N.; Yu, B.; Wen, M.; Wang, X.; Chu, P. K.; Yu, X. F. In-Plane Black Phosphorus/Dicobalt Phosphide Heterostructure for Efficient Electrocatalysis. Angew. Chem. Int. Ed. 2018, 57, 2600-2604.

S5. Yuan, Z. K.; Li, J.; Yang, M. J.; Fang, Z. S.; Jian, J. H.; Yu, D. S.; Chen, X. D.; Dai, L. M. Ultrathin Black Phosphorus-on-Nitrogen Doped Graphene for Efficient Overall Water Splitting: Dual Modulation Roles of Directional Interfacial Charge Transfer. J. Am. Chem. Soc. 2019, 141, 4972-4979.

S6. Liu, D.; Wang, J.; Lu, J.; Ma, C.; Huang, H.; Wang, Z.; Wu, L.; Liu, Q.; Jin, S.; Chu, P. K.; Yu, X.-F. Direct Synthesis of Metal-Doped Phosphorene with Enhanced Electrocatalytic Hydrogen Evolution. Small Methods 2019, 1900083.

S7. Zhu, X. D.; Xie, Y.; Liu, Y. T. Exploring the Synergy of 2D MXene-Supported Black Phosphorus Quantum Dots in Hydrogen and Oxygen Evolution Reactions. J. Mater. Chem. A 2018, 6, 21255-21260.